

Nuclear structure of ^{195}Pt

D. D. Warner, R. F. Casten, and M. L. Stelts*
Brookhaven National Laboratory, Upton, New York 11973

H. G. Börner and G. Barreau†
Institute Laue-Langevin, 38042 Grenoble, France

(Received 29 June 1982)

The level structure of ^{195}Pt has been investigated via a study of the $^{194}\text{Pt}(n,\gamma)^{195}\text{Pt}$ reaction. Secondary γ rays have been measured with curved crystal spectrometers and Ge(Li) detectors, and average resonance capture measurements have been performed to establish a complete set of low spin negative parity states below 1500 keV. The positive parity states reveal a decoupled band structure based on the $\frac{13}{2}^+$ isomer at 259 keV. The number of $J^\pi = \frac{1}{2}^-, \frac{3}{2}^-$ states identified below 1 MeV, a total of 11, indicates that a simple Nilsson model description will not be adequate to describe the observed level scheme. The negative parity structure is discussed in the framework of the interacting boson fermion approximation in light of the recently proposed multi- j supersymmetry predictions for this region.

NUCLEAR REACTIONS $^{194}\text{Pt}(n,\gamma)$, $E_n = \text{th}$, 2 keV, 24 keV; measured E_γ , I_γ ; ^{195}Pt deduced levels, J , π . Curved crystal spectrometers, Ge(Li) detectors, enriched targets. Comparison with predictions of multi- j supersymmetry in interacting boson-fermion approximation.

I. INTRODUCTION

A successful interpretation of the characteristics of odd mass nuclei depends critically on a valid description of the underlying core motion. In regions where the equilibrium nuclear shape is changing rapidly, such as the Pt-Os nuclei, the correct choice for such a description is not clear. Certainly, the use of either of the two simplest limiting descriptions involving the assumption of spherical or symmetrically deformed core structures is unlikely to prove adequate. It has recently been shown¹ that in the framework of the interacting boson approximation (IBA),² the structure of the even mass nuclei in this region corresponds to that expected near the O(6) limit of the model. More specifically, in considering the structure of ^{195}Pt , the appropriate core nucleus is ^{196}Pt , which is known to exhibit properties very close to the rigorous O(6) symmetry.³ Thus a study of ^{195}Pt offers the opportunity to investigate the accompanying boson-fermion formalism (IBFA) in a case where the core structure can be described analytically. One of the most crucial tests of this, or any other, formalism must be the establishment of a one-

to-one correspondence between the predicted and empirical level structure: The theory must account for the complete set of observed levels, and no more. The experimental technique most capable of providing the necessary guarantee of completeness, at least for low spin states, is the (n,γ) reaction,⁴ and while the states of ^{195}Pt have been well studied via radioactive decay⁵ and single nucleon transfer,^{6,7} no information on the low lying level structure has yet been obtained from (n,γ) studies.

The present study, therefore, presents the results of a number of (n,γ) studies of ^{195}Pt , thereby establishing a complete set of $J^\pi = \frac{1}{2}^-, \frac{3}{2}^-$ states below 1500 keV in excitation energy. Specifically, primary γ -ray transitions have been studied using the average resonance capture (ARC) technique at Brookhaven National Laboratory (BNL), while secondary γ rays have been studied with the high resolution curved crystal spectrometers at the Institut Laue-Langevin (ILL), and with Ge(Li) detectors at both laboratories. The high precision of the curved crystal data allows the Ritz combination principle to be used with confidence in constructing the level scheme, and the ARC data provide information on J^π assignments, as well as the crucial

guarantee that all low lying $J^\pi = \frac{1}{2}^-, \frac{3}{2}^-$ states have been observed. The resulting level scheme then offers an excellent basis for comparison with the predictions of any theoretical treatment of the nuclei in this region. In particular, it can be compared with the recent prediction⁸ of a multi- j supersymmetry in the IBFA framework.

II. EXPERIMENTAL TECHNIQUES

A. Curved crystal spectrometer measurements

The target for the curved crystal measurements consisted of 67 mg of platinum metal, enriched to 97.4% in ^{194}Pt . The material was pressed into a laminar form, and placed at a distance of 55 cm from the core of the High Flux Reactor at the Institut Laue-Langevin, Grenoble, in a thermal neutron flux of $5.5 \times 10^{14} \text{ cm}^{-2} \text{ s}^{-1}$, where it was viewed as a vertical line source by the curved crystal spectrometers, GAMS 1, GAMS 2, and GAMS 3. These instruments operate on the principle of Bragg diffraction from the (110) planes in quartz crystals, the diffracted γ rays being detected, after collimation, by a heavily shielded NaI detector. The diffraction angle is measured with high precision by laser-based Michelson interferometer systems, and for a given angular setting, five orders of reflection are recorded simultaneously. The GAMS 1 spectrometer was used for γ rays with energies below 400 keV, while the GAMS 2 and GAMS 3 spectrometers were used for the energy range 300–1000 keV. Further details of these instruments have been given elsewhere.⁹

B. Ge(Li) measurements

The low energy γ -ray spectrum from the $^{194}\text{Pt}(n,\gamma)^{195}\text{Pt}$ reaction was studied with Ge(Li) detectors at both the BNL and ILL reactors. At the ILL a sample of 110 mg of Pt metal (enriched to 97.4% in ^{194}Pt) was loaded in a graphite cylinder and mounted in the GAMS target position, 55 cm from the reactor core. The emerging γ -ray beam, after collimation, was viewed by a 20% coaxial Ge(Li) detector with a resolution of 2.1 keV at 1.33 MeV. The energy calibration was performed using contaminant lines from the $^{195}\text{Pt}(n,\gamma)^{196}\text{Pt}$ and $^{35}\text{Cl}(n,\gamma)^{36}\text{Cl}$ reactions, the energies being taken from the GAMS study and the data of Ref. 10.

At BNL the spectrum was studied at a quartz filtered thermal neutron beam. The target consisted

of 1.588 g of enriched ^{194}Pt metal. The data were taken with a 7% Ge(Li) detector, with typical resolution of 2.1 keV at 1.33 MeV, and recorded using an 8192 channel Northern analog-to-digital converter (ADC) interfaced through CAMAC to a PDP11/20-based data acquisition system. The ADC was stabilized against both zero and gain drifts using a precision double pulser. Energy and efficiency calibrations were obtained using a composite source of ^{182}Ta and ^{230}Th .^{11,12}

A γ - γ coincidence measurement was also performed at BNL using the detector described above, and a second 7% Ge(Li) detector coupled to an identical ADC/stabilizer system. The target and neutron beam used were those described in the singles measurement. The timing channel consisted of two Ortec constant fraction discriminators feeding a time-to-amplitude converter, the output of which was recorded in a third 256 channel ADC. Data were recorded in event mode, and analyzed on line to form the spectra in coincidence with the selected peak and background gates in one energy channel, and with true and accidental gates in the time channel.

C. Average resonance capture measurements

The intensities of primary γ rays feeding final states following thermal neutron capture are expected to be statistically distributed, following a Porter-Thomas distribution¹³ with one degree of freedom. Thus, all final states of a given J^π value may not be populated and those that are will be fed with widely varying strengths. The technique of average resonance capture (ARC) overcomes these disadvantages by employing a neutron beam with a broad width in energy. This results in a significant increase in the number of resonances contributing to the capture process, with a consequent decrease in the fluctuations of primary intensities. Given a sufficient number of resonances encompassed by the spread in beam energy, these fluctuations can be reduced to the point where *all* states of a given J^π value will be populated with close to equal primary intensity, after taking into account an energy factor which has been empirically determined as E_γ^5 .

The facility at BNL provides neutron beams with energies centered at 2 or 24 keV, the FWHM being approximately 0.85 and 1.9 keV, respectively. The beams are produced using Sc and ^{56}Fe filters, and full details are given elsewhere.¹⁴ Primary γ rays, in the energy range 5–8 MeV, were detected using a three crystal pair spectrometer, and a stabilized 8192 channel ADC. The target consisted of 41.7 g

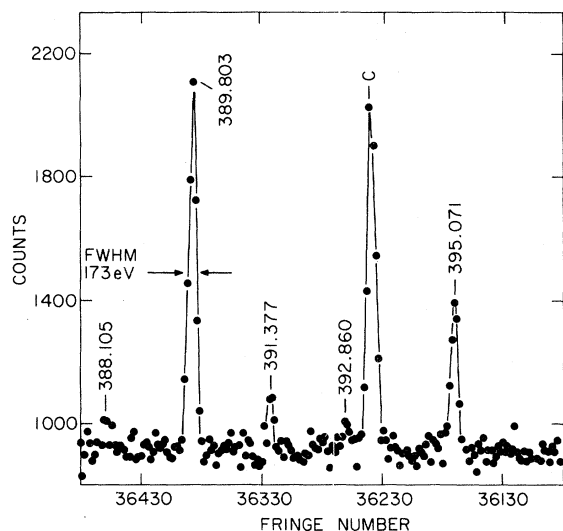


FIG. 1. A portion of the spectrum observed with the curved crystal spectrometer GAMS 2 in the second order of reflection. The peak labeled C is a contaminant from the $^{195}\text{Pt}(n,\gamma)^{196}\text{Pt}$ reaction.

of Pt enriched to 97.4% in ^{194}Pt . Nonlinearity and efficiency calibrations were obtained in a separate run with a thermal beam and a target of NaCl, using the results of Ref. 15.

III. RESULTS

A. Low energy γ -ray measurements

Portions of the spectra from the GAMS 2 spectrometer and from the Ge(Li) measurements are shown in Figs. 1 and 2. The low thermal neutron capture cross section (1.2 b) of the target nucleus

^{194}Pt resulted in an upper limit of about 700 keV for detection of lines with the curved crystal spectrometers, for which the efficiency falls off rapidly (as E_γ^{-2}) in this region. Detection of γ rays above this energy therefore relied on the Ge(Li) measurements. The allocation of lines to the $^{194}\text{Pt}(n,\gamma)^{195}\text{Pt}$ reaction was made by demanding consistent energies and relative intensities between the Ge(Li) measurements at ILL and BNL, and the curved crystal measurements at ILL, the three measurements having involved different target configurations and background environments. The final list of energies and intensities of all lines assigned to ^{195}Pt is given in Table I. The intensities were obtained from the BNL Ge(Li) data, after applying a correction for absorption in the target. Energies, where possible, were taken from the GAMS data, the absolute energy scale having been established by reference to the $K\alpha_2$ line of Pt at 65.122 keV. Energies for the weaker, higher energy lines were taken from the Ge(Li) data.

B. γ - γ coincidence measurements

The spectrum in coincidence with the 173 keV gate, after subtraction of background and accidental contributions, is shown in Fig. 3. No peaks other than those shown in Fig. 3 appeared in this spectrum up to 2 MeV. The peak at ≈ 338 keV is the result of backscattered 511 keV γ rays, and the negative peak on the high energy side stems from the subtraction of similar events in coincidence with a background gate set on the low energy side of the 173 keV line.

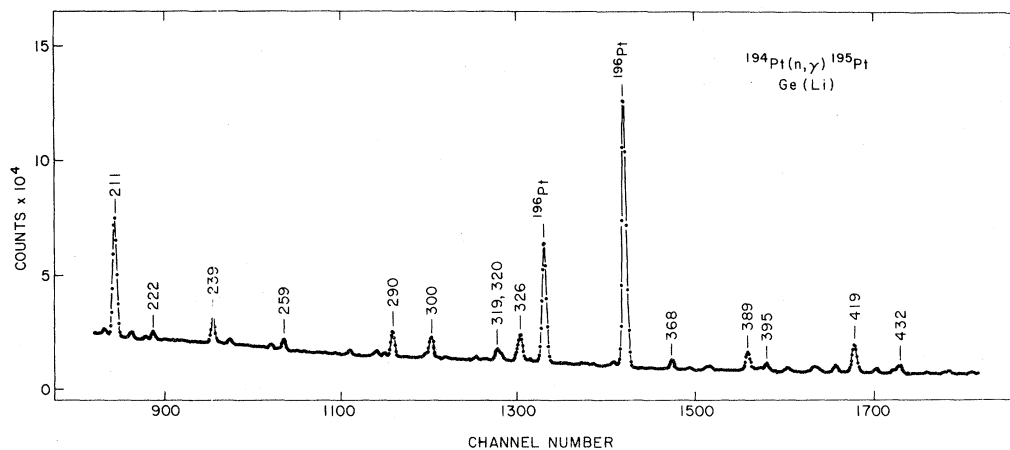


FIG. 2. A portion of the low energy singles spectrum taken with a Ge(Li) detector at BNL. The dominant peaks from the $^{194}\text{Pt}(n,\gamma)^{195}\text{Pt}$ reaction are labeled with their approximate energies in keV.

TABLE I. Gamma rays assigned to the $^{194}\text{Pt}(n, \gamma)^{195}\text{Pt}$ reaction.

γ -ray energy (keV) ^a	I_γ (rel) ^b	Assignment ^c		γ -ray energy (keV) ^a	I_γ (rel) ^b	Assignment ^c	
		Initial	Final			Initial	Final
98.886(2)	599(60)	98	0	432.647(22)	48(13) ^d	821	389
100.652(3)	131(13)	199	98	452.799(16)	40(5)	664	211
123.337(10)	130(13)	222	98	464.674(7)	60(7)	664	199
140.385(9)	115(16)	239	98	472.217(20)	53(12) ^e		
172.906(3)	505(51)	431	259	524.846(4)	186(19)	524	0
197.479(14)	50(9)	419	222	531.263(23)	40(12) ^d	630	98
199.533(2)	265(26)	199	0	533.252(19)	52(8) ^d		
211.407(2)	1000	211	0	534.418(15)	46(9) ^d	664	129
216.012(9)	52(6)	455	239	544.126(15)	40(5)		
222.230(5)	64(8)	222	0	590.895(7)	159(16)	590	0
239.261(5)	215(22)	239	0	594.264(35)	46(10) ^e		
243.855(14)	45(5)	455	211	612.870(21)	70(8)		
255.741(30)	39(5)	455	199	617.71(14)	21(4)		
259.351(6)	105(12)	389	129	629.86(25)	11(3)	630	0
285.578(4)	60(7)	524	239	635.589(31)	39(5)	1160	524
287.822(15)	37(4)			640.33(16)	20(3)	739	98
290.254(3)	290(29)	389	98	647.485(12)	75(8)		
299.114(12)	37(4)			687.686(56)	44(8)	926	239
300.811(2)	232(23)	1122	821	688.96(24)	30(8)		
313.449(6)	33(4)	524	211	705.07(13)	31(5)	1160	455
319.313(4)	82(9) ^d			715.11(14)	26(4)	926	211
319.843(4)	73(9) ^d	739	419	738.27(2)	30(6)		
320.819(3)	79(9) ^d	419	98	739.74(16)	41(6)	739	0
325.404(8)	90(12)			758.49(31)	17(5)		
328.471(10)	28(4)			776.709(50)	29(4)		
356.395(14)	66(12) ^e	455	98	864.19(38)	19(7)		
368.671(3)	146(15)	590	222	892.57(26)	19(5)	1132	239
373.459(9)	27(3)			913.93(43)	27(11)		
378.129(9)	47(6)	507	129	915.32(40)	37(10)		
379.503(8)	46(6)	590	211	917.13(29)	27(7)		
388.105(32)	26(4)			926.85(23)	25(7)	926	0
389.803(4)	309(31)	821	431	929.14(40)	25(8)		
391.377(10)	26(4) ^d	590	199	930.74(46)	22(7)		
392.860(19)	18(4) ^d	1132	739	948.70(15)	38(6)	1160	211
395.071(3)	134(15)	524	129	1005.60(8)	101(11)		
407.910(12)	60(7) ^d	630	222	1024.91(19)	28(5)		
409.049(11)	54(6) ^d	507	98	1030.60(22)	27(6)	1160	129
409.716(21)	54(7) ^d			1033.13(22)	29(6)	1132	98
414.327(6)	120(12)			1046.93(9)	113(12)		
418.741(8)	66(10)	630	211	1049.09(20)	37(6)		
419.705(4)	485(49)	419	0	1061.45(10)	86(10)	1160	98
420.711(60)	14(6)	1160	739	1064.82(50)	14(6)		
424.944(18)	18(5)	664	239	1066.77(23)	34(6)		
425.978(7)	72(8)	524	98	1076.04(21)	33(7)		
430.620(10)	63(7)	630	199	1091.27(8)	126(14)		
432.408(11)	108(16) ^d						

^aEnergies of secondary γ rays observed with GAMS spectrometers and Ge(Li) detectors at thermal neutron energies. Errors on the last digits are given in parentheses. The absolute calibration error is not included.

^bRelative γ -ray intensities, obtained from the Ge(Li) data and normalized to 1000 for the 211 keV transition.

^cNominal energies in keV of initial and final states between which the transition is placed.

^dTotal intensity of the multiplet was taken from the Ge(Li) data, while relative intensities of the individual components were obtained from the GAMS measurements.

^eThe γ ray was obscured in the Ge(Li) measurements by a contaminant. The intensity was obtained from the ratio in the GAMS spectra to neighboring lines.

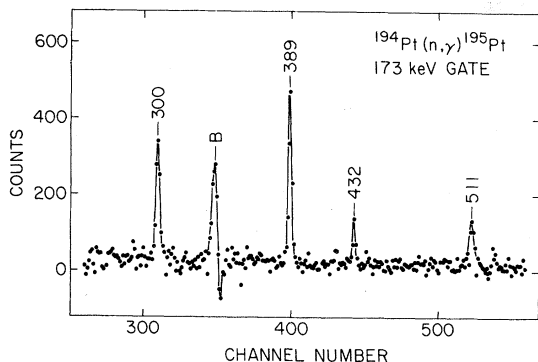


FIG. 3. A portion of the final Ge(Li)-Ge(Li) coincidence spectrum in coincidence with the 172.9 keV γ ray. No additional peaks, other than those shown, were found. Peaks are labeled with their approximate energies in keV. The structure labeled *B* at ≈ 338 keV results from backscattered 511 keV radiation, the negative portion corresponding to the selected background gate.

C. Average resonance capture measurements

A portion of the spectrum of primary γ rays following average resonance capture using the 2 keV neutron beam is shown in Fig. 4. Peaks are labeled by the nominal excitation energies of corresponding final states in ^{195}Pt . The thermal neutron binding energy was deduced to be 6105.3 ± 0.5 keV. This is in good agreement with the value deduced from a thermal primary measurement at ILL,¹⁶ and can be compared with the previous value of 6109.1 ± 2.9 of Wapstra and Bos.¹⁷

As mentioned in the preceding section, in considering the relative strengths of primary transitions it

has been found necessary¹⁸ to introduce an energy factor of E_γ^5 . A plot of the resultant reduced intensities from 2 keV capture is given in Fig. 5. The few resonances known in ^{195}Pt (Ref. 19) indicate an average energy spacing of ≈ 100 eV. This number, coupled with the 850 eV full width of the neutron beam, implies that the fluctuations in primary intensities should be reduced to the level of $\pm 48.5\%$. The two horizontal dashed lines on the figure show the band of intensities resulting from this spread, and it can be seen that most of the experimental points fall within the band, and thus correspond to *E1* primary transitions feeding final states with J^π values of $\frac{1}{2}^-$ or $\frac{3}{2}^-$, since *s*-wave capture will dominate at 2 keV neutron energy. The three points well below the band are then candidates for *M1* transitions to $\frac{1}{2}^+$, $\frac{3}{2}^+$ final states, since *M1* primary transitions are typically a factor of 6 lower in intensity.¹⁸ The dashed curve at the bottom of the figure indicates the sensitivity limit of the measurement, and it can be seen that it is very unlikely that any $\frac{1}{2}^-, \frac{3}{2}^-$ states below 1500 keV excitation energy could have been missed. Thus, it can be stated that any levels below 1500 keV *not* populated in this measurement must have J^π values *other* than $\frac{1}{2}^-, \frac{3}{2}^-$.

The final results of both the 2 and 24 keV measurements are summarized in Table II. In the case of 24 keV capture, a greater proportion of *p*-wave capture can be expected and hence the strength of primaries feeding $\frac{1}{2}^+, \frac{3}{2}^+$ states will be enhanced relative to the 2 keV data. The ratio of 2:24 keV reduced intensities thus gives an indication of the parity of the final state. In addition, $\frac{5}{2}^+, \frac{5}{2}^-$ states

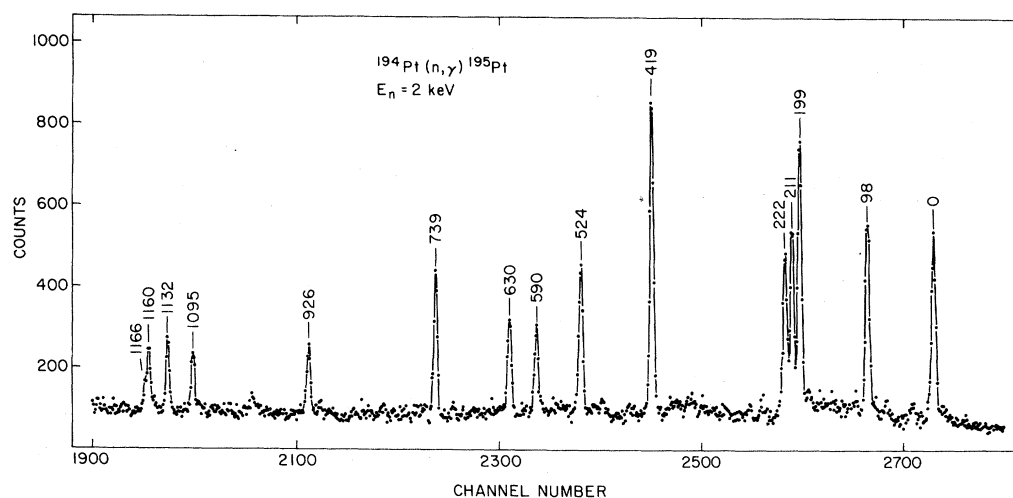


FIG. 4. The spectrum of double escape peaks from the average resonance capture experiments at 2 keV neutron energy. Peaks are labeled by nominal excitation energy in keV.

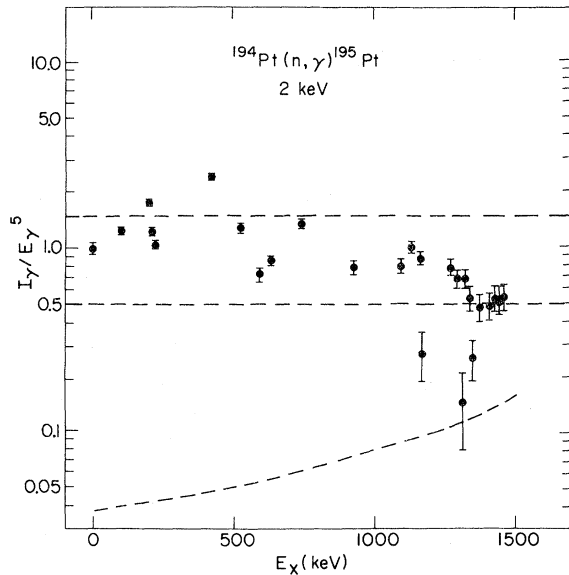


FIG. 5. Intensities (divided by E_γ^5) of the primary transitions from the $^{194}\text{Pt}(n, \gamma)^{195}\text{Pt}$ reaction at 2 keV neutron energy. The dashed horizontal lines represent the expected fluctuations in the maximum intensity ($J^\pi = \frac{1}{2}^-, \frac{3}{2}^-$) group. The curved dashed line at the bottom indicates the approximate sensitivity limit of the measurement.

can be populated by $E1$ ($M1$) transitions following p -wave capture, while such states would not be expected to be seen in the 2 keV measurement. These criteria, which are summarized in detail at the bottom of the table, led to the J^π assignments in the final column.

IV. LEVEL SCHEME

The high precision of the GAMS measurements of secondary γ rays allowed the Ritz combination technique to be used to confirm the existence of levels identified from the ARC and/or earlier data. The adopted levels and spin assignments up to 1500 keV in energy are summarized in Table III, and the associated decay scheme up to 1160 keV is shown in Fig. 6, the latter energy being limited by the sensitivity of the secondary γ -ray data. It should be noted that a number of additional levels of higher spin below 1160 keV are known from previous studies of the β decay from ^{195}Ir ,⁵ and in particular, from the $38\text{ h } \frac{11}{2}^-$ isomeric state in that nucleus. It can be seen from Table III that almost all of the adopted levels are supported by observation in either the current ARC or earlier single neutron transfer studies.⁶ The only exception is the 389.1 keV level,

which, however, was established in an earlier Coulomb excitation study.²⁰ In fact, no other levels below 1200 keV can be found from application of the Ritz combination technique, which involve the placement of more than 2 γ rays. The precise final energies listed in Table III result from use of the program LEVFIT,²¹ which makes a least squares fit to the measured transition energies.

The J^π assignments for the negative parity levels result largely from the ARC results, which as mentioned previously, provide the complete set of $J^\pi = \frac{1}{2}^-, \frac{3}{2}^-$ states. The $J^\pi = \frac{1}{2}^-$ possibility has been eliminated in a number of cases where earlier studies indicate an $E2$ component in the corresponding ground state transition, since the ground state of ^{195}Pt is known to have $J^\pi = \frac{1}{2}^-$ from atomic beam measurements.²² The unique $J^\pi = \frac{5}{2}^-$ assignments have been made on the basis that the ARC data show that these states cannot have $J^\pi = \frac{1}{2}^-, \frac{3}{2}^-$, while earlier conversion electron studies⁵ indicate either $E2$ transitions to the ground state, or $M1/E2$ transitions to the $\frac{3}{2}^-$ state at 98.9 keV. The $J^\pi = \frac{5}{2}^-, \frac{7}{2}^-$ assignments result from similar, though less restrictive, arguments. In all cases, the deduced J^π values are consistent with the l values assigned in the (d, p) and (d, t) studies, as evident in Table III.

The positive parity states require further comment. The spin of the isomeric state at 259.1 keV has been established as $\frac{13}{2}^+$ from nuclear orientation studies,²³ as well as from the $l=6$ transfer observed in the (d, t) and (p, d) work. The feeding of this level from the 432.0 keV state by the 172.9 keV γ ray has also been well established previously.⁵ The current coincidence study, with the 172.9 keV transition as gate, reveals an isolated set of three strong transitions of energies 389.8, 300.8, and 432 keV in coincidence. It was not possible to determine which member of the doublet at 432 keV was seen in the coincidence experiment. However, the former two transitions combine with the 432.0 keV level energy to yield levels at 821.8 and 1122.6 keV whose energies are consistent with two positive parity states populated in the 24 keV ARC measurement. The previous decay studies favored a $J^\pi = \frac{11}{2}^+$ assignment for the 432 keV level, due to the observation of an $M1$ component in the 172.9 keV transition. However, the (d, t) and (p, d) studies indicated an $l=4$ transfer suggesting a $\frac{9}{2}^+$ assignment. The current work resolves this question unambiguously, since the maximum spin possible for the 821.8 keV from the ARC data is $\frac{5}{2}^+$. Thus the spin of the 432.0 keV level must be $\frac{7}{2}^+$. The

TABLE II. High energy γ rays in ^{195}Pt observed in 2 and 24 keV capture. M represents a multiplet which contained several contaminant lines as well as the quoted primary γ rays, and all the components could not be completely resolved. Our best estimates for the energies and intensities of the primary transitions are quoted.

E_x^a	2 keV		24 keV		$\frac{I_R(2\text{ keV})^c}{I_R(24\text{ keV})}$	J^{π^f} ARC
	$E(\Delta E)^b$	I_γ/E_γ^{5c}	$E(\Delta E)^b$	I_γ/E_γ^{5c}		
0.0	6106.8(3)	100(6)	6129.5(4)	100(7)	1.00	$\frac{1}{2}^-, \frac{3}{2}^-$
98.9(3)	6008.2(3)	124(6)	6030.7(4)	111(9)	1.11	$\frac{1}{2}^-, \frac{3}{2}^-$
199.6(3)	5907.7(3)	175(7)	5929.8(4)	108(9) M	1.61	$\frac{1}{2}^-, \frac{3}{2}^-$
211.4(3)	5895.8(3)	123(6)	5916.7(12)	105(25) M	1.18	$\frac{1}{2}^-, \frac{3}{2}^-$
222.2(3)	5885.0(3)	105(7)	5907.9(9)	169(20) M	0.62	$\frac{1}{2}^-, \frac{3}{2}^-$
419.8(3)	5687.5(3)	242(7)	5709.6(5)	89(9)	2.72	$\frac{1}{2}^-, \frac{3}{2}^-$
454.8(9)			5674.7(9)	28(9)	0	$\frac{5}{2}^\pm$
524.9(3)	5582.4(3)	127(7)	5604.3(4)	138(11)	0.92	$\frac{1}{2}^-, \frac{3}{2}^-$
590.8(3)	5516.6(4)	72(6)	5538.5(6)	68(10)	1.06	$\frac{1}{2}^-, \frac{3}{2}^-$
630.1(3)	5477.2(3)	85(6)	5499.0(5)	76(11)	1.12	$\frac{1}{2}^-, \frac{3}{2}^-$
739.4(3)	5368.2(3)	134(7)	5389.1(5)	75(11)	1.79	$\frac{1}{2}^-, \frac{3}{2}^-$
821.7(8)			5307.8(8)	44(11)	0	$\frac{5}{2}^+, (\frac{5}{2}^-, \frac{1}{2}^+, \frac{3}{2}^+)$
926.8(4)	5180.4(4)	78(7)	5204.5(13)	46(16)	1.70	$\frac{1}{2}^-, \frac{3}{2}^-$
1095.8(4)	5012.0(4)	79(7)	5033.2(5)	113(16)	0.70	$\frac{1}{2}^-, \frac{3}{2}^-$
1121.3(9)			5008.2(9)	55(17)	0	$\frac{5}{2}^+, (\frac{5}{2}^-, \frac{1}{2}^+, \frac{3}{2}^+)$
1132.6(4)	4974.6(4)	100(7)	4997.9(11)	42(14)	2.38	$\frac{1}{2}^-, \frac{3}{2}^-$
1160.3(4)	4946.7(6)	86(9)	4969.5(6)	140(19)	0.61	$\frac{1}{2}^-, \frac{3}{2}^-$
1166.4(6)	4940.8(12)	27(8)	4963.1(7)	96(17)	0.28	$\frac{1}{2}^+, \frac{3}{2}^+$

432 keV coincident transition cannot be placed in the scheme of Fig. 6, but presumably feeds the cascade from a higher level. The absolute energies of the set of positive parity states, shown in Table III and Fig. 6, are based on the placement of the 432.6 keV transition deexciting the 821.8 level, which links the energies of the positive parity states to the negative parity set. If this placement is chance, the positive parity energies would have to be based on the previously determined energy of the $\frac{13}{2}^+$ isomer, which was 259.4 ± 0.2 keV.

V. DISCUSSION

A. Positive parity structure

In considering the positive parity states the only shell model orbit available near the Fermi surface in ^{195}Pt is the $i_{13/2}$ orbit. Nevertheless, the population of a $\frac{13}{2}^+$ isomer in an (n, γ) reaction with a capture

state spin of $\frac{1}{2}^+$ is in itself a striking feature. The mechanism for such population was revealed by the results of the coincidence spectrum gated by the 172.9 keV transition, which had previously been placed as feeding the $\frac{13}{2}^+$ state at 259.1 keV. These data reveal a $\frac{5}{2}^+, \frac{9}{2}^+, \frac{13}{2}^+$ decoupled band structure, which, in terms of a Nilsson model analysis, would indicate an oblate potential in which the Fermi surface is near the low K $i_{13/2}$ Nilsson orbits. Similar structures have been identified in the lighter mass Pt nuclei.²⁴ The assumption of an oblate potential for the odd mass Pt nuclei would seem to be not inconsistent with the known structure of the corresponding even-even nuclei, whose potential surfaces are thought to exhibit both oblate and prolate minima of roughly equal depth, with a high degree of γ softness. The empirical observations mentioned above would then indicate that the odd particle induces a greater dominance of the oblate

TABLE II. (Continued.)

E_x^a	2 keV		24 keV		$\frac{I_R(2\text{ keV})^e}{I_R(24\text{ keV})}$	J^π^f ARC
	$E(\Delta E)^b$	I_γ/E_γ^{5c}	$E(\Delta E)^b$	I_γ/E_γ^{5c}		
1271.0(3)	4836.3(4)	78(8)	4858.3(6)	115(20)	0.68	$\frac{1}{2}^-, \frac{3}{2}^-$
1287.7(4)	4819.6(5)	67(8)	4841.5(7)	107(18)	0.63	$\frac{1}{2}^-, \frac{3}{2}^-$
1312.7(7)	4795.0(15)	15(7)	4816.7(8)	82(21)	0.18	$\frac{1}{2}^+, \frac{3}{2}^+$
1320.8(4)	4786.6(5)	68(8)	4808.3(6)	107(20) ^d	0.64	$\frac{1}{2}^-, \frac{3}{2}^-$
1334.7(4)	4772.5(5)	53(8)	4795.1(9)	72(19)	0.74	$\frac{1}{2}^-, \frac{3}{2}^-$
1346.9(6)	4760.2(9)	26(7)	4782.7(8)	82(22)	0.32	$\frac{1}{2}^\pm, \frac{3}{2}^\pm$
1372.7(4)	4734.6(5)	47(8) ^d	4756.5(9)	77(19)	0.61	$\frac{1}{2}^-, \frac{3}{2}^-$
1411.1(5)	4696.0(6)	48(8)	4718.7(9)	71(23)	0.68	$\frac{1}{2}^-, \frac{3}{2}^-$
1425.0(5)	4682.2(6)	53(9)	4704.4(9)	78(25)	0.68	$\frac{1}{2}^-, \frac{3}{2}^-$
1438.3(4)	4669.7(7)	52(9)	4690.8(5)	157(35) ^d	0.33	$\frac{1}{2}^\pm, \frac{3}{2}^\pm$
1445.3(5)	4662.0(6)	54(9) ^d	4683.9(9)	99(23)	0.54	$\frac{1}{2}^-, \frac{3}{2}^-$

^aExcitation energy in keV. Errors on the last digits are in parentheses. The energy quoted is the weighted mean of the value obtained from the 2 and 24 keV data.

^bEnergy of γ ray in keV. Errors on the last digits are in parentheses.

^cIntensity of γ ray, divided by the fifth power of the γ -ray energy. These reduced intensities are given in arbitrary units, and normalized to a value of 100 for the primary transition feeding the ground state in each measurement. Errors on the last digits are in parentheses.

^dIntensity corrected for contribution from contaminant.

^eRatio of the reduced primary intensities observed in 2 and 24 keV capture. The reduced intensities are defined in c.

^fSpin and parity assignments which could be made from the ARC data alone. The following convention was adopted:

$$\begin{aligned}
 I_R(2\text{ keV})/I_R(24\text{ keV}) > 0.5 & J^\pi = \frac{1}{2}^-, \frac{3}{2}^- \\
 0.3-0.5 & \frac{1}{2}^\pm, \frac{3}{2}^\pm \\
 < 0.3 & \frac{1}{2}^+, \frac{3}{2}^+ \\
 0 & \frac{5}{2}^+ (\frac{5}{2}^-, \frac{1}{2}^+, \frac{3}{2}^+) \text{ for } I_R(24\text{ keV}) > 30 \\
 & \frac{5}{2}^\pm \text{ for } I_R(24\text{ keV}) < 30.
 \end{aligned}$$

minimum in these nuclei. However, it is in fact very unlikely that a Nilsson potential, as such, can account for the structure of these nuclei, since such a potential assumes an axially symmetric oblate deformation, i.e., the disappearance of the effects of the competing prolate minimum in the potential surface. Indeed, the limitations on the use of the simple Nilsson potential in this region become particularly evident when the negative parity structure is considered, as will be seen below. Nevertheless, the use of a more realistic core description will not necessarily lead to problems in the description of the observed positive parity structure, since it has been shown²⁵ that a structure resembling a decoupled band can result from a core particle coupling calculation involving a core which is not rotational.

B. Negative parity structure: Comparison with the predictions of a multi- j supersymmetry

It is thus crucial to consider the negative parity structure in ¹⁹⁵Pt. The most striking feature, evident in Fig. 1, is the large number of $J^\pi = \frac{1}{2}^-, \frac{3}{2}^-$ levels below 1 MeV, a total of 11. Many of these have been identified for the first time in the current study, including the level at 222 keV, thus showing the advantages of the nonselective nature of the (n, γ) reaction. The negative parity shell model orbits available in ¹⁹⁵Pt are the $p_{3/2}$, $f_{5/2}$, and $p_{1/2}$, and thus a maximum of eight states with $J^\pi = \frac{1}{2}^-, \frac{3}{2}^-$ can be formed by coupling these to a deformed core represented by a ground state rota-

TABLE III. Properties of levels below 1500 keV in ^{195}Pt .

GAMS E_x (ΔE_x)	ARC E_x (ΔE_x)	Previous work ^a		J^π ^b
		E_x	l	
0	0	0	1	$\frac{1}{2}^-$
98.884(2)	98.9(3)	98.9	1	$\frac{3}{2}^-$
129.782(3)		129.7	3	$\frac{5}{2}^-$
199.533(2)	199.6(3)	199.6	1	$\frac{3}{2}^-$
211.406(2)	211.4(3)	211.3	1	$\frac{3}{2}^-$
222.230(3)	222.2(3)			$\frac{1}{2}^-$, $\frac{3}{2}^-$
239.267(3)		239.3	3	$\frac{5}{2}^-$
259.075(22)		259.2	6	$\frac{13}{2}^+$
389.136(3)		389.2		$\frac{5}{2}^-$
419.704(3)	419.8(3)			$\frac{3}{2}^-$
431.980(22)		432.0	(4)	$\frac{9}{2}^+$
		449.7	}	$(3)^c$
455.274(7)	454.8(9)	455.2		
507.919(7)		507.9		
524.850(3)	524.9(3)	524	1	$\frac{3}{2}^-$
		539		$\frac{1}{2}^-$
		547.0		
		562.6		
590.901(3)	590.8(3)			$\frac{1}{2}^-$, $\frac{3}{2}^-$
		612.7	3	
630.147(6)	630.1(3)			$\frac{1}{2}^-$, $\frac{3}{2}^-$
664.206(6)		663		$\frac{5}{2}^-$, $\frac{7}{2}^-$
		695.2	(3)	
739.546(5)	739.4(3)	738.9	1	$\frac{1}{2}^-$, $\frac{3}{2}^-$
		765.8	3	
		793		
		814.6	(5)	

tional band. Since this is the assumption implicit in the simple Nilsson model, such an approach cannot describe the data and, as suggested initially, a more realistic core description must be included. Attempts to include the effects of the low lying second 2^+ core state have already been made,⁶ in which, in the framework of an oblate Nilsson potential, the states at 0 and 211.4 keV were assigned as the first two members of the $\frac{1}{2}^-$ [530] band, and the 98.9 keV state was taken as the $\frac{3}{2}^-$ [532] bandhead. However, while the state at 199.5 keV was assigned as the $\frac{3}{2}^-$ [541] bandhead, its energy could not be well reproduced because of the Coriolis interaction with the $\frac{1}{2}^-$ [530] band. Thus the identification of another $J^\pi = \frac{1}{2}^-, \frac{3}{2}^-$ state at 222.2 keV in the current study provides further evidence that a more complete core description is required.

As pointed out in the Introduction, the formalism of the interacting boson-fermion approximation

offers an ideal basis within which to study the structure of ^{195}Pt . Moreover, the ability to describe the ^{196}Pt core structure analytically, in terms of the O(6) limit of the model, is a particular advantage. However, recent theoretical developments have revealed an even more intriguing possibility. It was previously shown²⁶ that, in the case of bosons with O(6) symmetry, coupled to a fermion in a $j = \frac{3}{2}$ orbit, the collective and single particle degrees of freedom could be described together in a single analytic framework which resulted in the prediction of a supersymmetry, applicable to both the even-even and odd-even nuclei. Some empirical evidence of this symmetry^{27,28} was found from studies centered on the odd-proton (e.g., Au and Ir) nuclei in this region, where the $d_{3/2}$ proton orbit is near the Fermi surface and the only competing orbit extraneous to the theoretical supersymmetry is the $s_{1/2}$ orbit. While some indications suggestive of this

TABLE III. (Continued.)

GAMS E_x (ΔE_x)	ARC E_x (ΔE_x)	Previous work ^a		J^π ^b
		E_x	l	
821.784(22)	821.7(8)	821.9		$\frac{5}{2}^+$
		875		
		895.4		
		915		
926.947(54)	926.8(4)	927.7	1	$\frac{1}{2}^-, \frac{3}{2}^-$
		930.7		
		971.3	3	
		1049.3		
	1095.8(4)	1098	1	$\frac{1}{2}^-, \frac{3}{2}^-$
1122.594(22)	1121.3(9)			$\frac{5}{2}^+ (\frac{3}{2}^-, \frac{1}{2}^+, \frac{3}{2}^+)$
1132.400(20)	1132.6(4)			$\frac{1}{2}^-, \frac{3}{2}^-$
1160.384(25)	1160.3(4)	1159	(3,4)	$\frac{1}{2}^-, \frac{3}{2}^-$
	1166.4(6)			$\frac{1}{2}^+, \frac{3}{2}^+$
	1271.0(3)			$\frac{1}{2}^-, \frac{3}{2}^-$
	1287.7(4)	1294	1	$\frac{1}{2}^-, \frac{3}{2}^-$
	1312.7(7)			$\frac{1}{2}^+, \frac{3}{2}^+$
	1320.8(7)			$\frac{1}{2}^-, \frac{3}{2}^-$
	1334.7(4)	1337		$\frac{1}{2}^-, \frac{3}{2}^-$
	1346.9(6)			$\frac{1}{2}^\pm, \frac{3}{2}^\pm$
	1372.7(4)			$\frac{1}{2}^-, \frac{3}{2}^-$
	1411.1(5)			$\frac{1}{2}^-, \frac{3}{2}^-$
	1425.0(5)	1420	(1)	$\frac{1}{2}^-, \frac{3}{2}^-$
	1438.3(4)			$\frac{1}{2}^\pm, \frac{3}{2}^\pm$
	1445.3(5)	1445		$\frac{1}{2}^-, \frac{3}{2}^-$

^aThe data are taken from Table II of Ref. 6 which includes the data of Ref. 5. The best values for E_x and l obtainable from the (d,p) , (d,t) , and decay studies are quoted.

^bFinal spin assignments from the current study. See text for a detailed discussion.

^cUnresolved peak in the (d,p) and (d,t) studies.

$d_{3/2} \times O(6)$ supersymmetry were found, it was difficult to empirically extract, with confidence, the subset of levels involving an odd proton in specifically this one orbit.

More recently, however, it has been demonstrated⁸ that a more complex class of supersymmetry can be constructed, which incorporates $j = \frac{1}{2}, \frac{3}{2}$, and $\frac{5}{2}$ single particle orbits coupled to the $O(6)$ boson core. This situation then corresponds to the negative parity orbits available to the odd neutron nuclei in this region ($p_{3/2}, f_{5/2}, p_{1/2}$). In this case, there are *no other* nearby orbits which can perturb the expected structure, so that the purity of the $O(6)$

symmetry exhibited by ^{196}Pt implies that ^{195}Pt should offer perhaps the best chance of observing this new class of supersymmetries. In fact, it has already been suggested⁸ that the current results represent the first empirical evidence for this new symmetry.

In the notation of Ref. 8, the boson-fermion system forms the group structure $U^{(B)}(6) \times U^{(F)}(12)$, where the fermion part describes the three available single particle levels $j = \frac{1}{2}, \frac{3}{2}$, and $\frac{5}{2}$. Then, if the boson part can be described by the $O(6)$ symmetry, an analytic expression results for the eigenvalues of the combined system, namely

$$\begin{aligned}
 E(\Sigma; (\sigma_1, \sigma_2, \sigma_3); (\tau_1, \tau_2); L; J) = & -\frac{A}{4} \Sigma(\Sigma + 4) - \frac{A''}{4} [\sigma_1(\sigma_1 + 4) + \sigma_2(\sigma_2 + 2) + \sigma_3^2] \\
 & + \frac{B}{6} [\tau_1(\tau_1 + 3) + \tau_2(\tau_2 + 1)] + CL(L + 1) + C''J(J + 1). \quad (1)
 \end{aligned}$$

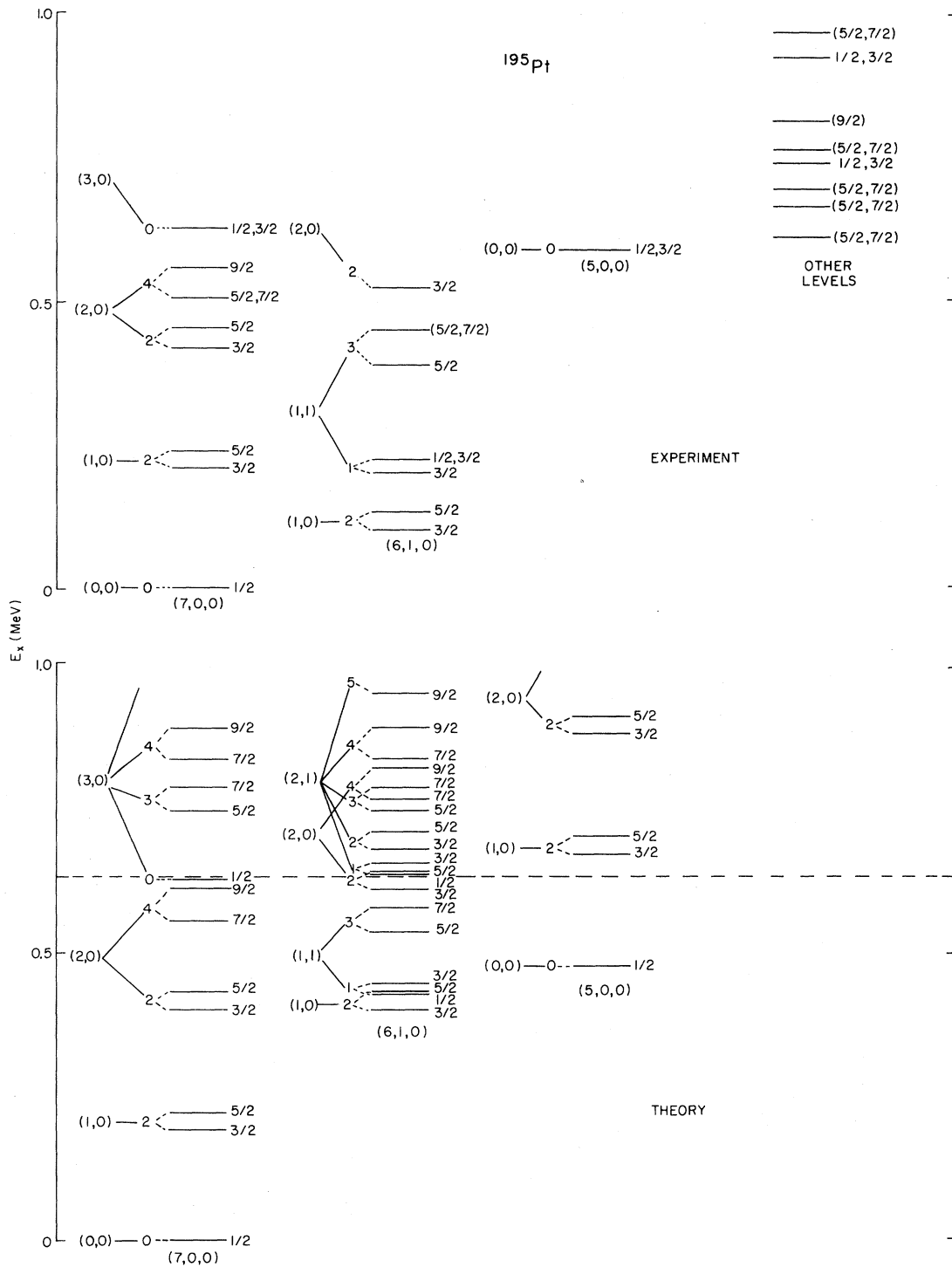


FIG. 7. Comparison of the empirical negative parity levels in ^{195}Pt with the predictions of the multi- j supersymmetry of Ref. 8. Parameter values of $A''/4=15$ keV, $B/6=35$ keV, and $C=C'=6$ keV were used in Eq. (1). The levels are labeled on the left with the quantum numbers $(\tau_1, \tau_2)-L$, and below with $(\sigma_1, \sigma_2, \sigma_3)$. The dashed line across the lower scheme indicates the limit of excitation energy up to which a one-to-one correspondence has been suggested (Ref. 8) between theoretical and experimental levels.

theory accounts for the complete set of $J^\pi = \frac{1}{2}^-, \frac{3}{2}^-$ states established below this energy, and does not predict any additional states. In addition, the theory can account for the known states of higher spin, and while these cannot be guaranteed complete, so that in a number of cases, states are predicted which have not been observed to date, there are no negative parity states known empirically which do not fit into the predicted structure below this energy. There also seems to be empirical evidence for the predicted occurrence of $J = L + \frac{1}{2}, L - \frac{1}{2}$ pairs of states based on a particular value of the pseudo-orbital angular momentum L , with separations proportional to $J(J+1)$. Thus there are three proposed $J^\pi = \frac{3}{2}^-, \frac{5}{2}^-$ couplets which have approximately constant energy spacing. Note that this spacing is too small (≈ 30 keV) in all cases, relative to the energy of the first 2^+ state in the neighboring even nuclei, to be consistent with a simple rotational band structure.

It is instructive at this stage to attempt to extend the correspondence between theory and experiment to higher excitation energies. To this end, the complete sets of empirical and predicted levels up to 1 MeV are included in Fig. 7. It can be seen that the theory now predicts *too many* $J^\pi = \frac{1}{2}^-, \frac{3}{2}^-$ states. Specifically, the $(\tau_1, \tau_2) = (2, 1)$ states of the (610) group involve three additional $J^\pi = \frac{1}{2}^-, \frac{3}{2}^-$ states. It would clearly be purely speculative to attempt a correspondence between theory and experiment at these higher energies. However, it is interesting to note that, without the $(\tau_1, \tau_2) = (2, 1)$ states, it would be possible to continue the one-to-one correspondence up to 1 MeV.

At this point, it should be emphasized that the association between empirical and theoretical states suggested in Fig. 7 has been largely based on energies and spins, and thus cannot be considered conclusive. The only exception is the $\frac{3}{2}^-, \frac{5}{2}^-$ multiplet of the (610) configuration where $B(E2)$ data were taken into account (see below). It is clearly necessary to extensively compare predicted and empirical transition probabilities and single particle transfer cross sections in order to confirm the proposed assignments. Unfortunately, a detailed description of the selection rules for $E2$ and $M1$ transitions, and (d, p) and (d, t) cross sections, associated with the multi- j supersymmetry, has not yet been given. Preliminary studies²⁹ indicate that for $E2$ transitions, the selection rules governing transitions from the representations with $\sigma_2 = \sigma_3 = 0$ should be identical to those applicable in the even mass core, namely, $\Delta(\sigma_1, \sigma_2, \sigma_3) = 0$ and $\Delta(\tau_1, \tau_2) = (1, 0)$. For

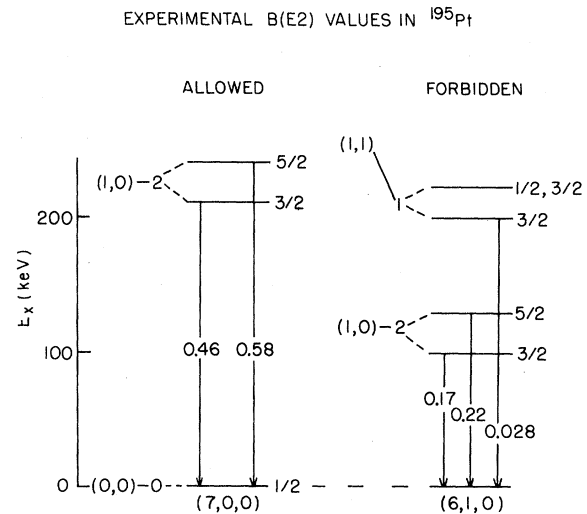


FIG. 8 Empirical $B(E2)$ values in ^{195}Pt . The numbers on the arrows are in units of e^2b^2 . The suggested quantum numbers are indicated as in Fig. 7.

the $(6, 1, 0)$ representation, the rule is $\Delta(\tau_1, \tau_2) = (1, 0)$ or $(0, 1)$, implying that τ_1 and τ_2 cannot change simultaneously. In general, a transition operator in the IBFA formalism will involve a boson part and a fermion part. The above selection rules will result when the $E2$ operator is a generator of the combined group. However, when there is no specific relationship between the two parts, the σ selection rule is relaxed and becomes $\Delta(\sigma_1, \sigma_2, \sigma_3) = (1, 1, 0)$ or $(0, 0, 0)$. For $E2$ transitions, where the collective part of the operator is likely to dominate, the first, more rigorous selection rule is likely to hold. However, the relative γ -ray intensities measured in the current, and earlier, studies cannot be used to investigate the degree to which the predicted selection rule is valid since in most cases, an $M1$ component is possible, and the $E2/M1$ mixing has not been determined. Theoretically, the $M1$ selection rule is likely to be similar to the second case described above involving a possible change in σ as well as τ quantum numbers, since the operator will be dominated by the fermion part.

Nevertheless, there are some Coulomb excitation data²⁰ which provide empirical $B(E2)$ values for a few of the lower states, and these are displayed in Fig. 8. The selection rule $\Delta(\tau_1, \tau_2) = (1, 0)$ implies that only two states should be populated directly in such studies, those at 211 and 239 keV. It is clear from Fig. 8 that while these are indeed the dominant empirical $B(E2)$ values, there is also some population of the $(\tau_1, \tau_2) = (1, 0)$ states in the $(6, 1, 0)$ group, indicating a degree of symmetry breaking.

The actual $B(E2)$ values for the 211 and 239 keV states are 0.46(3) and 0.58(3) e^2b^2 , respectively, which can be compared with the $B(E2;0^+ \rightarrow 2^+_{1-})$ value in ^{196}Pt of 1.32(6) e^2b^2 .³⁰ Assuming that the core contribution dominates in the odd mass nucleus, these numbers indicate that 79% of the expected $E2$ strength is found in the two “allowed” states, and thus may provide a measure of the extent to which the rigorous symmetry is broken. In addition, it can be seen that the remaining strength is accounted for by the transitions to the 99 and 129 keV states.

The origin and effects of the symmetry breaking can be considered in more detail. As in the even mass [O(6)] case, the primary effects of such breaking should be manifested as mixing between the different σ representations. If the breaking is not large, the τ quantum numbers should remain relatively pure. There is some evidence to suggest that this is indeed the case. In Fig. 7, it can be seen that the proposed (7,0,0) and (5,0,0) σ groups agree reasonably well in energy with the predicted structures. On the other hand, the (6,1,0) group is considerably perturbed. This might be expected since the (6,1,0) group can interact via σ -mixing terms with both the (5,0,0) and (7,0,0) groups. The empirical $B(E2)$ values of Fig. 8 reinforce these ideas. The only “forbidden” transitions with significant strength are those to the levels at 99 and 129 keV. These two states correspond to the $(\tau_1, \tau_2) = (1,0)$ states of the (6,1,0) group. The $B(E2)$ strength to the 199 keV state, with $(\tau_1, \tau_2) = (1,1)$, is an order of magnitude weaker, indicating that the τ quantum numbers may still be relatively pure.

VI. SUMMARY AND CONCLUSIONS

The current study has provided a considerable amount of new information concerning the states and transitions in the ^{195}Pt level scheme. The positive parity structure resembles that of a decoupled band based on the $i_{13/2}$ state. The majority of low lying states have negative parity, and a complete set of $J^\pi = \frac{1}{2}^-, \frac{3}{2}^-$ states has been established, up to an excitation energy of 1500 keV. The large number of these states below 1 MeV indicates that a successful theoretical interpretation must incorporate a rather complete description of the underlying core motion. In general, the guarantee of completeness provided by the current results, and the subsequent conclusions which can be drawn from such a guarantee, emphasize the importance of the nonselective nature of the (n, γ) reaction in the study of nuclear structure.

The preliminary comparison of the ^{195}Pt level scheme with the recent predictions of a multi- j supersymmetry shows promising agreement. Perhaps the most impressive feature is the possibility to establish a one to one correspondence between the low lying negative parity states in theory and experiment. In this respect, the current results must offer a challenge to other theoretical approaches in this region of nuclei. They also point to the likelihood of there being a similarly large number of as yet unidentified $J^\pi = \frac{1}{2}^-, \frac{3}{2}^-$ states in neighboring odd mass Pt nuclei. In order to investigate this possibility, average resonance capture studies have been made of ^{197}Pt and ^{199}Pt , and these results will be reported soon.

Despite the successful overall reproduction of the low lying level structure observed in ^{195}Pt , it must be reiterated that the degree to which the supersymmetry is manifested empirically cannot be firmly established until further studies are made, both experimental and theoretical, concerning the relative $E2$ and $M1$ transition probabilities, and the single particle transfer cross sections. The existing $B(E2)$ data for the low lying levels point to a breaking of the symmetry at the level of $\approx 20\%$. However, examination of the predictions in the 600–1000 keV region indicates that the rigorous supersymmetry predicts too many low spin states. It would be instructive to reproduce the supersymmetry in the framework of the general IBFA Hamiltonian of Ref. 31, and then to investigate the symmetry breaking terms which must be introduced to obtain better agreement with the data. While it is not immediately obvious that the formalism of the general Hamiltonian will permit the generation of the supersymmetry, recent work³² proposes a connection between the constants in the eigenvalue expression of Eq. (1) and the relative sizes of the terms in the general Hamiltonian.

In conclusion, the current data may offer the first detailed example of this new class of supersymmetries, involving more than one j -orbital. If further studies confirm the proposed association of empirical and theoretical states, and the relatively small symmetry breaking suggested by the existing $B(E2)$ data, this new formalism offers the opportunity to provide a relatively simple explanation of the complex structure of negative parity states in the odd mass nuclei in this region.

This research was performed under Contract DE-AC02-76CH00016 with the U.S. Department of Energy.

- *Current address: Los Alamos National Laboratory, Physics Department, Los Alamos, NM 87545.
- †Current address: C. E. N. Bordeaux-Gradipnau, 33170 Gradipnau, France.
- ¹R. F. Casten and J. A. Cizewski, Nucl. Phys. A309, 477 (1978).
- ²A. Arima and F. Iachello, Ann. Phys. (N.Y.) 99, 253 (1976); 111, 201 (1978); 123, 468 (1979).
- ³J. A. Cizewski, R. F. Casten, G. J. Smith, M. L. Stelts, W. R. Kane, H. G. Borner, and W. F. Davidson, Phys. Rev. Lett. 40, 167 (1978).
- ⁴R. F. Casten, D. D. Warner, M. L. Stelts, and W. F. Davidson, Phys. Rev. Lett. 45, 1077 (1980).
- ⁵J. F. W. Jansen, A. Faas, and W. J. B. Winter, Z. Phys. 261, 95 (1973).
- ⁶Y. Yamazaki and R. K. Sheline, Phys. Rev. C 14, 531 (1976).
- ⁷G. R. Smith, N. J. Di Giacomo, M. L. Munger, and R. J. Peterson, Nucl. Phys. A290, 72 (1977).
- ⁸A. B. Balentekin, I. Bars, R. Bijker, and F. Iachello, Yale Report No. YTP82-11; F. Iachello, in Proceedings of the 1982 INS International Symposium on Dynamics of Nuclear Collective Motion, Mt. Fuji, Japan, 1982 (unpublished).
- ⁹H. R. Koch, H. G. Borner, J. A. Pinston, W. F. Davidson, J. Faudou, R. Rousille, and O. W. B. Schult, Nucl. Instrum. 175, 401 (1980).
- ¹⁰A. M. J. Spits and J. Kopecky, Nucl. Phys. A264, 63 (1976).
- ¹¹D. H. White, R. E. Birkett, and T. Thomson, Nucl. Instrum. 77, 261 (1970).
- ¹²V. Zobel, J. Eberth, U. Eberth, and E. Eube, Nucl. Instrum. 141, 329 (1977).
- ¹³C. E. Porter and R. G. Thomas, Phys. Rev. 104, 483 (1956).
- ¹⁴M. L. Stelts and J. C. Browne, Nucl. Instrum. 133, 35 (1976).
- ¹⁵M. L. Stelts and R. E. Chrien, Nucl. Instrum. 155, 253 (1978).
- ¹⁶C. Hoffmeyer, private communication.
- ¹⁷A. Wapstra and K. Bos, At. Data Nucl. Data Tables 19, 177 (1977).
- ¹⁸L. M. Bollinger and G. E. Thomas, Phys. Rev. Lett. 18, 1143 (1967).
- ¹⁹S. F. Mughabghab and D. I. Garber, Brookhaven National Laboratory Report BNL-325, 1973.
- ²⁰W. T. Milner, F. K. McGowan, R. L. Robinson, P. H. Stelson, and R. O. Sayer, Nucl. Phys. A177, 1 (1971).
- ²¹K. Schreckenbach, program LEVFIT.
- ²²Gladys H. Fuller, J. Phys. Chem. Ref. Data 5, 835 (1976).
- ²³F. Bacon, G. Kaindl, H.-E. Mahnke, and D. A. Shirley, Phys. Rev. Lett. 28, 720 (1972).
- ²⁴M. Piiparinen, J. C. Cunnane, P. J. Daly, C. L. Dors, F. M. Bernthal, and T. L. Khoo, Phys. Rev. Lett. 34, 110 (1975).
- ²⁵G. Alaga and V. Paar, Phys. Lett. 61B, 129 (1976).
- ²⁶F. Iachello and S. Kuyucak, Ann. Phys. (N.Y.) 136, 19 (1981).
- ²⁷J. L. Wood, in *Interacting Bose-Fermi Systems in Nuclei*, edited by F. Iachello (Plenum, New York, 1981), p. 381.
- ²⁸J. A. Cizewski, D. G. Burke, E. R. Flynn, Ronald E. Brown, and J. W. Sunier, Phys. Rev. Lett. 46, 1264 (1981).
- ²⁹F. Iachello, private communication.
- ³⁰H. H. Bolotin, I. Katayama, H. Sakai, Y. Fujita, M. Fujiwara, K. Hosono, T. Itahashi, T. Saito, S. H. Sie, P. Conley, D. L. Kennedy, and A. E. Stuchbery, J. Phys. Soc. Jpn. 47, 1397 (1979).
- ³¹F. Iachello and O. Scholten, Phys. Rev. Lett. 43, 679 (1979).
- ³²R. Bijker, private communication.